Regular Articles

Designing hollow-core multi-mode anti-resonant fibers for industrial high-power laser delivery

William Shere [*], Gregory T. Jasion, Eric Numkam-Fokoua, Francesco Poletti

Optoelectronics Research Centre, University of Southampton, Southampton SO171TA, United Kingdom

ABSTRACT

We investigate the design of hollow-core fibers for the delivery of 10s of kilowatt average power from multi-mode laser sources where delivery through solid-core fibers is typically limited by nonlinear optical effects to 10s of metres of distance. A technique is presented for the design of multi-mode anti-resonant fibers that can efficiently capture and deliver light from these lasers. We analyze, by numerical simulation, the performance of two anti-resonant fibers designed using this technique to target lasers with M^2 up to 13 and find they are capable of delivering MW-level power over multi-kilometres distances with low leakage loss, and at bend radii as small as 35 cm. Pulsed lasers are also investigated and numerical simulations indicate that optimized fibers could in principle deliver nanosecond pulses with pulse energy greater than 100 mJ over more than 1 km. This would be orders of magnitude higher power and longer distances than in typical machining applications using state-of-the-art solid core fibers.

1. Introduction

Hollow-core anti-resonant fibers (ARF) have been the subject of remarkable and rapid progress in recent years which has proven the theoretical promise of the technology [1,2]. The first tubular fibers were reported fabricated in 2011 with losses in the order of a few dB/m [3]. Just nine years later, in 2020 a nested anti-resonant nodeless fiber (NANF) was reported with 0.28 dB/km loss at telecommunication wavelengths, only marginally higher than solid-core silica fiber [4]. In 2021 a NANF targeting shorter wavelengths achieved the all-time record low-loss transmission in any type of optical fiber e.g. 0.3 dB/km at 1060 nm [5]. More recently in 2022 the first double-nested anti-resonant nodeless fiber (DNANF) was reported with attenuation of 0.174 dB/km at 1550 nm on par with that of commercial solid-core single-mode fibers [6]. With the performance of these fibers now proven and further loss reduction still possible, the focus of research is turning to applications that can exploit their low non-linearity, latency and dispersion [7], exceptional polarization purity [8], ultralow backscattering [9] and low loss.

The unique benefits of ARF make high-power laser delivery a promising application area. Solid-core fibers are primarily limited in maximum power and delivery distance by the onset of nonlinear processes [10]. The maximum power distance product before stimulated Raman scattering significantly modifies the signal is given by $P \cdot L_{\text{eff}} = 16 A_{\text{eff}}/g_r$, where P is the laser power, L_{eff} is the effective interaction length of the fiber, A_{eff} is the effective interaction area and g_r is the

Raman gain coefficient (for a large core, multi-mode silica fiber $L_{\text{eff}} \approx L$ when $L < 100$ m, $A_{\text{eff}} \approx \pi(0.8R)^2$ and $g_r = 1 \times 10^{-13}$ m W^{-1}) [11]. To allow delivery of increasingly higher power lasers, solid-core fibers must have a commensurate increase in core size and so large-mode-area or large-core, multi-mode fibers are typically employed. Transmission of 1 kW of power over 100 m has been reported in a highly multi-mode (~750 modes) step-index fiber [12] and 10 kW over 30 m has been demonstrated in a three-mode photonic crystal fiber [13]. Commercially available solutions are typically limited to a few 10 s of metres e.g. the delivery fiber of a commercial multi-mode 10 kW fiber laser is up to 30 m long and has 100 μm core diameter [14]. Compared to solid-core fibers, ARFs intrinsically exhibit greatly reduced optical nonlinearity since more than 99.99% of light is guided in air [7,15] for which the nonlinear coefficient is almost three orders of magnitude less than silica [16]. The properties of ARFs raise the potential for significant improvements in reach, flexibility and power handling capabilities compared to solid-core fibers.

The past two decades have seen great progress in the practical demonstrations of laser power delivery through hollow-core fibers [17–22], culminating in the remarkable demonstration of 1 kW continuous-wave (CW) power transmitted over 1 km of single-mode NANF [23]. This body of work has so far focused on the transmission of high quality, single-mode laser beams with $M^2 \approx 1$. Greater laser power still is available from few-mode and multi-mode lasers [24], and there

* Corresponding author.
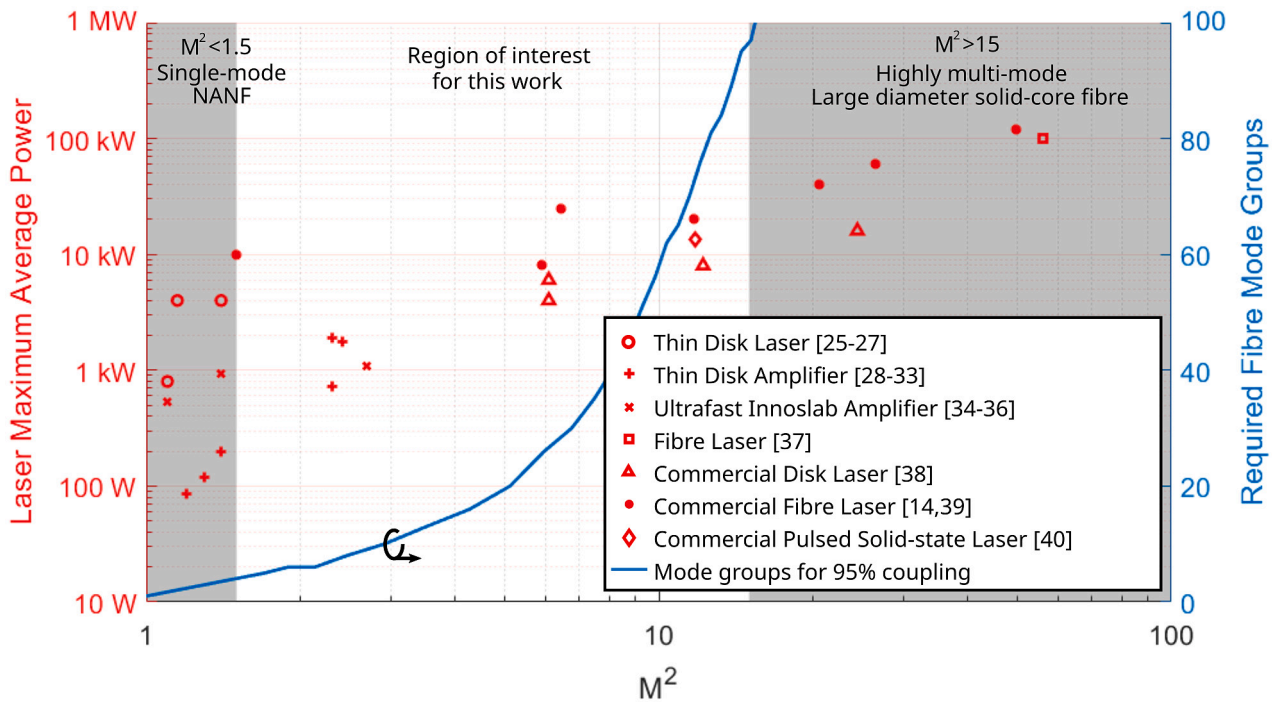 *E-mail address:* w.shere@soton.ac.uk (W. Shere).

Fig. 1. (red markers, left axis) The maximum average power output of high power laser sources and their reported M^2 values [14,25–40]. (blue line, right axis) the number of mode groups required to be guided in a hollow-core fiber to achieve 95% coupling efficiency for an incident laser beam of a given M^2. The laser described by [39] is characterized only as single-mode and a beam quality $M^2 = 1.5$ is assumed.

are a broad range of applications which would benefit from the ability to deliver such lasers across long distances using fibers. Also of interest are nearly single-mode lasers, e.g. $M^2 \approx 1.5$, which would suffer high insertion loss when coupled into a single-mode fiber. In Fig. 1 the red markers illustrate a representative selection of high-power lasers emitting near 1030 nm, commercially available or reported in literature, of various architectures, both pulsed and continuous wave (cw). Higher power lasers are increasingly multi-moded with output beam M^2 values increasingly approximately proportionally to the maximum average power [24]. To efficiently couple light from few- and multi-mode (MM) sources into a fiber requires a similarly few-mode or MM fiber. To quantify this we calculated the number of modes required to be guided in an ARF in order to capture at least 95% of the power from a laser beam with a given M^2. More details of this calculation are given in Section 2 where it is shown that this determination is approximately independent of the exact fiber design or laser transverse profile. The data is represented by the blue line on the left axis of Fig. 1. As suggested, lasers with larger M^2 values require more multi-mode fibers for efficient coupling and plotting the data in this manner allows for a simple approximation of the design requirements for a given laser. For example, the 9.8 kW fiber laser with $M^2 = 6$ would require an ARF guiding approximately 26 mode groups to achieve 95% coupling efficiency. Clearly, to exploit the high power-handling capabilities of ARF for applications requiring flexible delivery of optical power from high-power lasers over some distance, we must design low-loss ARFs that are multi-mode.

Considering the lasers currently available and the fiber requirements shown in Fig. 1, in this work we investigate ARFs for delivery of sources with M^2 values from 1.5 to 15 that corresponds to output average power up to 30 kW. This range is highlighted in Fig. 1. Nearly diffraction-limited lasers with $M^2 < 1.5$ are here considered approximately single-mode. The results of Mulvad et al. show that multi-kilowatt power can be delivered from single-mode lasers through single mode NANF over several kilometres. For example, in an air-filled NANF delivery of 5 kW over more than 2 km is predicted possible. Above the region of interest, $M^2 > 15$ laser sources can emit more

than 100 kW average power [37]. These lasers are highly multi-mode (ie. more than 100 mode groups) and fiber delivery is typically through highly multi-mode solid-core fibers with core diameters as large as 800 μm [14]. It is conceivable that ARFs might one day be designed to guide the several 100 s of mode groups required to efficiently couple light from these sources, however, it is not the focus of this work. We focus instead on the intermediate range $1.5 < M^2 < 15$ where MM ARFs can offer significant improvements on the performance of solid-core fibers.

2. Coupling of multi-mode laser beams into multi-mode ARFs

We first consider the case of a generic laser beam coupling into an optical fiber. A commonly used quantity for characterizing beam quality is the M^2 factor, defined as the ratio of the beam parameter product to that of the ideal, diffraction-limited Gaussian beam [41]. A beam with 100% of power in the fundamental Gaussian beam mode therefore has $M^2 = 1$ and this is the highest quality beam physically achievable. Greater M^2 values correspond to beams with larger divergence angles that have a fraction of the total power being transmitted by higher-order and higher-divergence modes. When coupling to a fiber, more power in higher-order beam modes causes the transverse profile of the beam to differ from the Gaussian-like fundamental fiber mode and therefore beams with higher M^2 will not couple efficiently into single-mode fiber. Instead multi-mode delivery fibers are required.

Highly multi-mode guidance is easily achieved in solid-core fibers and indeed is generally a natural consequence of scaling the core size to achieve the power-handling capabilities required by high-power lasers; a MM step-index fiber with numerical aperture 0.22 and core diameter 50 μm will guide several 100 s of modes and the larger cores typically used for high power delivery can guide many times more. The highly multi-mode nature of these fibers mean they can easily achieve efficient coupling for large M^2 beams. In hollow-core ARFs, however, the guidance mechanism results in strong differential properties between modes, with higher order modes generally exhibiting higher losses, higher dispersion and higher overlap with the glass [42]. Knowledge of the number of fiber modes required to accommodate a beam with a

given M^2 is therefore crucial in designing the fiber since guiding more modes than are required will likely reduce the fiber performance.

In this work we target the design of fibers enabling at least 95% coupling efficiency to a given MM laser source. This is the highest efficiency we are aware of being practically reported in ARF [43]. Any laser energy not coupled into the core may instead be absorbed by the fiber cladding or coating causing heating and potentially damage if not managed. A coupling efficiency of 95% should reduce the requirement for active cooling at the fiber coupling, enable high throughput and permit further power upscaling.

To calculate coupling efficiency we consider how the modes of an ARF are excited by an incident field. These modes form a complete, orthogonal set and are normalized such that for any mode labeled k and k':

$$\iint \vec{\mathbf{z}} \cdot (\mathbf{E}_k \times \mathbf{H}_{k'}^* + \mathbf{E}_{k'}^* \times \mathbf{H}_k)\, dA = \delta_{k,k'} \tag{1}$$

where $\mathbf{E}_k$, $\mathbf{H}_k$ are the electric and magnetic fields of the kth fiber mode and $\delta_{s,u}$ is the Kronecker delta, which evaluates to 1 if $s = u$ and 0 otherwise. Since the modes form a complete set, any incident field, $\mathbf{E}^{(i)}$ and $\mathbf{H}^{(i)}$, can be described as a linear combination of the modes:

$$\mathbf{E}^{(i)} = \sum_k c_k \mathbf{E}_k, \quad \mathbf{H}^{(i)} = \sum_k c_k \mathbf{H}_k \tag{2}$$

with c_k the amplitude coupling coefficient into mode k given by:

$$c_k = \iint \vec{\mathbf{z}} \cdot (\mathbf{E}^{(i)} \times \mathbf{H}_k^* + \mathbf{E}_k^* \times \mathbf{H}^{(i)})\, dA \tag{3}$$

If the incident field, $\mathbf{E}^{(i)}$ and $\mathbf{H}^{(i)}$, has been normalized according to Eq. (1) to carry unit power then $|c_k|^2$ describes the power coupling efficiency into mode k. In order to describe the transverse field of a non-unity M^2 laser beam we employ the Laguerre–Gaussian formulation which describes a free space laser mode as:

$$\mathbf{E}_l^{(LG)}(\rho, \phi) = \vec{\mathbf{t}} \cdot \left(\frac{\rho\sqrt{2}}{w_0}\right)^{|m_l|} \exp\left(-\frac{\rho^2}{w_0^2}\right) L_{n_l}^{|m_l|}\left(\frac{2\rho^2}{w_0^2}\right) \exp(-im_l\phi) \tag{4}$$

where $\vec{\mathbf{t}}$ is the electric field polarization vector, w_0 is the beam waist, m_l and n_l are the radial and azimuthal mode indices respectively of the lth Laguerre–Gaussian mode and $L_n^m(x)$ is the Laguerre polynomial. As with the modes of an ARF the Laguerre–Gaussian modes form a complete, orthogonal set and, given the normalization of Eq. (1), we can describe the emitted laser beam, as a linear sum of those modes:

$$\mathbf{E}^{(i)} = \sum_l c_l \mathbf{E}_l^{(LG)}, \quad \mathbf{H}^{(i)} = \sum_l c_l \mathbf{H}_l^{(LG)} \tag{5}$$

This description has the advantage that the M^2 value of a laser beam is obtained from its modal decomposition as [44]:

$$M^2 = \sum_l (1 + m_l + 2n_l)|c_l|^2 \tag{6}$$

For Eq. (6) to hold the beam must be propagating unit power, i.e. $\sum_l |c_l|^2 = 1$.

Beam quality is not sufficient to capture the transverse field profile; from Eq. (6) we can understand that different combinations of the same modes, i.e. beams with different transverse fields, can result in equal M^2. The black bars in Fig. 2(a–c) show three different modal distributions that all result in a laser beam with $M^2 = 3$. To determine how different transverse profiles affect coupling we show in the colored bars of Fig. 2(a–c) the modal coupling coefficients for a 10-mode-group fiber. Results are shown for a hollow, circular fiber (a circular air hole in bulk silica, see the $N = 0$ structure in Fig. 4). Distinct laser beams result in a distinct excitation of the fiber modes. Like-like mode groups tend to couple most strongly; the mode group in the fiber carrying the most power here always has the same order as whichever mode group in the laser beam carried the most power. Cross-coupling between modes of different order, however, generally results in power being spread between lower- and higher-order modes

in the fiber. In Distributions 1 and 3 there is negligible power outside of the first 5 mode groups of the laser but for both distributions, more than 10% of the power is captured by mode group 6 and above in the fiber. Fig. 2(d) shows, for all the previous beam distributions, the total coupling efficiency into the fiber as a function of the beam waist ratio. The beam waist ratio is defined as the ratio between the laser beam waist and the fiber core radius, w_0/R. Regardless of the exact modal distribution in the laser, the same number of fiber modes is capable of capturing >95% of the beam. The maximum difference between the distributions shown here is 5% but at the optimum beam waist ratio the discrepancy is less than 1% and generally the results are nearly identical across the entire range. This $M^2 = 3$ beam is optimally coupled at $w_0/R = 0.45$. It will be shown in Section 4.1 that beams with increased higher-order mode content are optimally coupled at smaller values of beam waist ratio.

Note that although only 3 distributions are shown here for clarity, throughout the preparation of this work, a range of input beams were investigated and we found that for all metrics we explored, M^2 is a robust measurement with beams of diverse modal composition and polarization but equal M^2 achieving similar fiber performance. Given the similarity between results, we henceforth use for the remainder of the paper the modal decomposition described by the parameters of Distribution 2 to generate beams of a desired M^2.

We next calculate the required number of mode groups a fiber must guide in order to achieve our target of 95% coupling efficiency with a given laser beam. We conducted numerical simulation, using the commercial finite-element solver COMSOL Multiphysics, of a range of ARF geometries including tubular, NANF and DNANF and, although the transverse mode profiles, $\mathbf{E}$ and $\mathbf{H}$, differ in each of these structures, all geometries exhibited nearly identical requirements on the number of mode groups. To allow the mode profiles to be determined analytically, we consider the modes of a hollow, circular fiber as determined by Marcatili and Schmeltzer [45]. In Fig. 1 we show the number of mode groups required to be guided in a fiber to achieve our target of 95% coupling efficiency for a given incident beam, characterized by its M^2 value. We find that a $M^2 = 3$ beam would require approximately 10 mode groups but the number of mode groups required to achieve the 95% coupling efficiency increases rapidly with M^2; an $M^2 = 10$ beam requires around 60 mode groups and $M^2 > 15$ requires more than 100 groups.

2.1. Coupling efficiency of HOMs in second anti-resonant window

In high-performance applications, when coupling power into an optical fiber, even a subtle increase in coupling efficiency can make a significant difference to the performance of that system. This is even more valid in high-power systems, where high coupling efficiency improves not only the power performance but also the safety of the system. It has been shown that in single-mode ARFs coupling efficiency can be improved by almost 2% by operating the fiber in the second anti-resonant window rather than the fundamental window [46]. Although the available optical bandwidth is reduced in the second anti-resonant window [7], an improvement to coupling efficiency is typically more important in high-power fiber delivery.

To investigate the possibility of improved coupling efficiency for multi-mode ARFs in the second anti-resonant window we simulated two NANFs with core radius $R = 35\,\mu m$, guiding 12 mode groups at wavelength $\lambda = 1030\,nm$. When considering anti-resonant windows it is useful to normalize the frequency. The normalized frequency is defined as:

$$F = \frac{2t}{\lambda}\sqrt{n_g^2 - 1} \tag{7}$$

for wavelength λ, wall thickness t and glass refractive index n_g [47]. High-loss resonances occur for integer values of F with low-loss anti-resonant windows in-between; the fundamental anti-resonant window exists for $0 < F < 1$, the second window $1 < F < 2$ etc.. For this
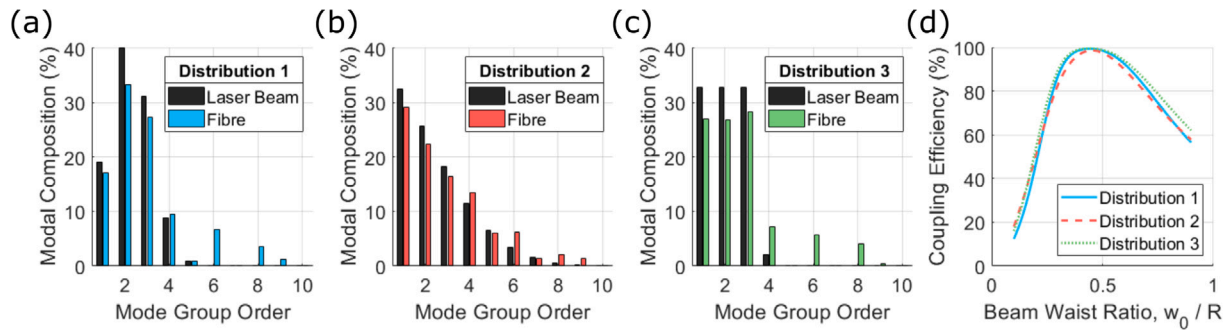
Fig. 2. (a–c) Several different modal distributions of (black bars) laser beams with $M^2 = 3$ before and (colored bars) after coupling into a fiber. (a) Distribution 1 and (b) Distribution 2 are described by discrete Gaussian functions with standard deviation 1 and 3 respectively and mean chosen to achieve the target M^2. (c) Distribution 3 is flat across lower order modes with the power of the highest order mode chosen to achieve the target M^2. (d) The total coupling efficiency of the beams described by (a–c) incident on a 10 mode fiber as a function of the beam waist ratio.
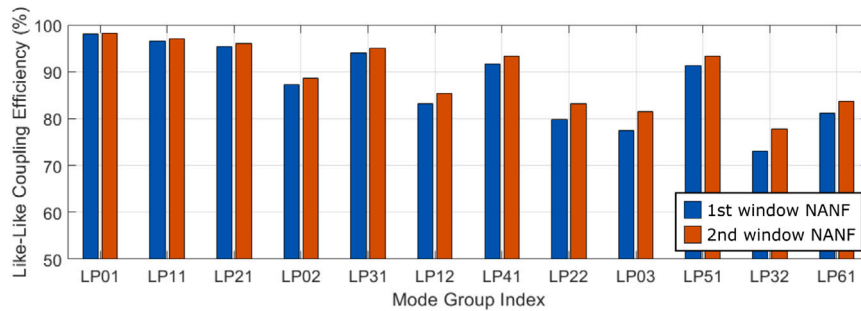

Fig. 3. The modal coupling efficiency of Laguerre–Gaussian laser modes into the same mode of a multi-mode NANF operating in either the fundamental (blue) or second anti-resonant window (red).
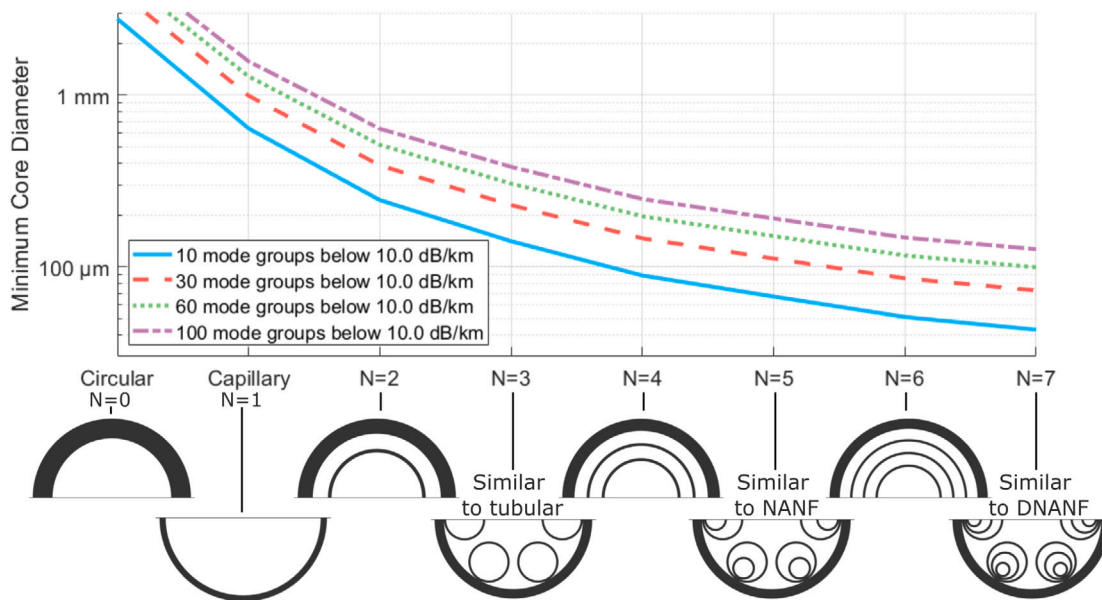

Fig. 4. The predicted minimum core size, according to Eq. (8), in order to guide 10, 30, 60 or 100 mode groups with a maximum loss less than 10 dB/km at 1030 nm for different ARF structures.

experiment we simulated NANFs with $t = 350$ nm and $t = 700$ nm respectively corresponding to a normalized frequency $F = 0.71$ in the fundamental window and $F = 1.42$ in the second window. The coupling efficiency was calculated between the fiber modes and their equivalent Laguerre–Gaussian laser modes, e.g. the LP_{01} fiber mode and the LP_{01} Laguerre–Gaussian mode. Fig. 3 shows this like-like modal coupling efficiency for the first and second window NANFs when the laser beam is focused to the optimal value for that mode. Both fibers have highest coupling efficiency in the fundamental LP_{01} mode

group, approximately 98%, which decreases for higher-order modes. The lowest coupling efficiency amongst the first 12 guided mode groups is, for both fibers, less than 78% in the LP_{32} mode group. Note that since the contribution of unlike modes (e.g. coupling from the LP_{01} laser mode group into the LP_{11} fiber mode group) is not included, Fig. 3 is not representative of overall coupling efficiency and is only meant to elucidate the effects of operating in different anti-resonant windows. As indicated by Fig. 2(c), for example, coupling between unlike modes contributes significantly to overall coupling efficiency.

Coupling efficiency decreases more rapidly with increasing radial mode order than azimuthal mode order. There is more than a 10% drop between the LP_{01} and LP_{02} mode groups and between the LP_{11} and LP_{12} groups, whereas between the LP_{01}, LP_{11} and LP_{21} mode groups the total drop in coupling efficiency is less than 3%. This suggests that the number of modes required in an optical fiber to achieve high coupling efficiency increases more rapidly than the number of modes in the incident laser beam. It should be stressed that a real multi-mode laser beam carries power in a some or all of these modes and optimal focusing will not be possible for all modes simultaneously.

When comparing the first and second window NANFs, higher coupling efficiencies are found in the second window NANF. Coupling efficiency in the highest order, LP_{61}, mode group is 2.5% greater in the second window NANF and the improvement is more than 4% in the lowest efficiency, LP_{32}, mode group. The increase in the fundamental mode however is less than 0.25%. In general, the improvements found by operating the fiber in the second anti-resonant window are minimal for the lowest-order modes and increase with mode order. This is understood by considering the mechanism for the increase in coupling efficiency, as reported in ref. [46]. The electric field of a mode operating in the fundamental window changes sign as it crosses the thin capillary separating the core and the cladding, i.e. it is positive in the core and negative (but with small magnitude) in the cladding. The mode field of a Gaussian beam is always positive and so the overlap integral (Eq. (3)) is reduced by the contribution of the cladding regions. By contrast, in the second anti-resonant window, the sign of the fiber mode changes twice when crossing the capillary wall and is therefore positive in the core and cladding. The overlap integral in a second-window NANF is increased by the cladding contribution. While the sign of the electric field of the fiber mode in the cladding determines whether there is a positive or negative contribution to the coupling efficiency, evidently it is the magnitude of the electric field in the cladding relative to the electric field in the core that determines how large the effect on the overlap integral is. For any guided mode in an ARF the amount of power propagating in the cladding increases as the loss of that mode increases [42]. This explains the results shown in Fig. 3; the highest-order mode have the highest loss and, therefore, have the highest fraction of power propagating in the cladding. As a result the highest-order modes exhibit a large increase in coupling efficiency when operating in the second anti-resonant window compared to the fundamental window whereas for the lowest-order modes the improvement is marginal.

For the multi-mode laser beams considered in this work, a significant fraction of power is coupled into low-order fiber modes, which exhibit marginal increase in coupling efficiency in the second anti-resonant window. When calculating the modal requirements of NANFs operating in the second anti-resonant window, therefore, there was a negligible improvement over NANFs operating in the fundamental anti-resonant window. Considering the wider bandwidth achievable in the fundamental anti-resonant window, for the remainder of this work only fundamental-window NANFs are studied. In the next section we discuss how the coupling requirements relate to design of anti-resonant fiber.

3. Multi-mode ARF design for high power laser delivery

In this section we present a design process for NANFs to guide the number of modes required to effectively capture and guide radiation from a multi-mode, high power laser. We derive a minimum core size requirement and describe how to design the cladding of a NANF to achieve multi-mode guidance.

3.1. Minimum core size

Unlike conventional solid-core fibers, the guidance mechanism of ARF results in high differential-loss between modes; a mode is considered guided if the loss of that mode is sufficiently low for the

intended application. Since, generally, the highest order mode will have the highest loss it is sufficient in multi-mode guidance to design the fiber such that the loss of the highest order mode is below a desired threshold [42].

Throughout this work we only consider losses due to confinement or leakage. Because of the large cores needed for multi-mode guidance, surface scattering remains negligible [7] and whilst microbending increases rapidly with core size [48,49], we speculate that these fibers could be packaged in such a way its contribution can also be negligible compared to leakage loss.

The designs of ARF of interest in this work cannot be modeled analytically. In this work we propose making an estimate of the loss as that of a similar, simpler ARF design. The leakage loss of a structure consisting of concentric rings of air and glass (see for example the $N = 6$ fiber of Fig. 4) has been determined in closed form by Bird. For such a structure the leakage loss in decibels per unit length is given by [50]:

$$\alpha = \frac{20}{\ln 10} \left(\frac{x_0}{2\pi} \right)^{N+2} \frac{\epsilon_r^{N+1} + 1}{2(\epsilon_r - 1)^{(N+1)/2}} \frac{\lambda^{N+2}}{R^{N+3}} \prod_{i=1}^{N} \frac{1}{\sin^2(\phi_i)} \quad (8)$$

with R the core radius, λ the wavelength and ϵ_r the relative dielectric constant of the glass regions. The variable x_0 is a number determined by the mode; for the HE_{mn} mode it is the nth zero of the Bessel function J_{m-1}. The geometry is characterized by N which is the integer number of finite concentric rings (including both air and glass regions) which make up the cladding (see Fig. 4 for examples). The final product term in Eq. (8) extends over the cladding regions and in this work we take $\phi_{glass} = 2\pi t \sqrt{\epsilon_r - 1}/\lambda$ and $\phi_{air} = \pi/2$. To target an operating wavelength of 1030 nm, we choose a membrane thickness $t = 350\,\text{nm}$ that corresponds to a normalized frequency, $F = 0.71$ (see Eq. (7)) such that 1030 nm is near the expected minimum loss of the fundamental anti-resonant window [47]. The choice of ϕ_{air} corresponds to an "optimal" width of the air regions in the concentric ring structure where leakage loss is minimal (see [50]). Whilst there is no simple equivalent concept of an optimal width of air regions in NANF, they have been demonstrated to have lower losses for the same core size than even the most optimal concentric ring structure [7].

Although Eq. (8) describes the loss of a concentric ring structure, in this work we use it to estimate the loss of tubular, NANF and DNANF geometries. These designs most closely resembles $N = 3$, 5 and 7 respectively [7,51]. Since tubular, NANF and DNANF designs typically have lower losses than similar concentric ring structures our estimate is expected to produce larger-than-necessary core sizes. As in solid-core fibers, ARFs with larger cores exhibit higher losses due to both macro- and micro-bending [49] and it may be therefore practically beneficial to introduce a scaling factor to correct for the discrepancy between geometries. In this work, however, we find our simple approximation sufficient, ensuring the performance of the fiber exceeds the design parameters. We will show that the macro-bending losses of these designs surpasses the typical requirements of industrial laser fiber delivery.

In this work we select a loss threshold of 10 dB/km for the highest-order guided mode and therefore the maximum, worst-case propagation loss over 100 m will be 1 dB. Fig. 4 shows, for a range of values of N, the minimum core diameter determined by Eq. (8), to guide 10, 30, 60 or 100 mode groups below this threshold. With reference to Fig. 1 this corresponds to efficiently capturing light from laser beams with $M^2 \leq$ 3, 7, 10 and 15. Eq. (8) suggests that tubular fibers with core diameters of 140 μm can support up to 10 low-loss mode groups, however, such a large core tubular fiber is expected to suffer from very severe bend loss which would make it unsuitable in this application [52]. The core size requirements of ARF designs with additional nested elements are greatly reduced. A NANF with core diameter 70 μm, half that of the tubular fiber, is predicted to guide 10 mode groups whilst a NANF with core diameter 150 μm can guide 60 mode groups. The bending resilience of NANFs is significantly improved compared to tubular fiber (e.g. loss is more than 4 orders of magnitude lower for 80 μm core diameter
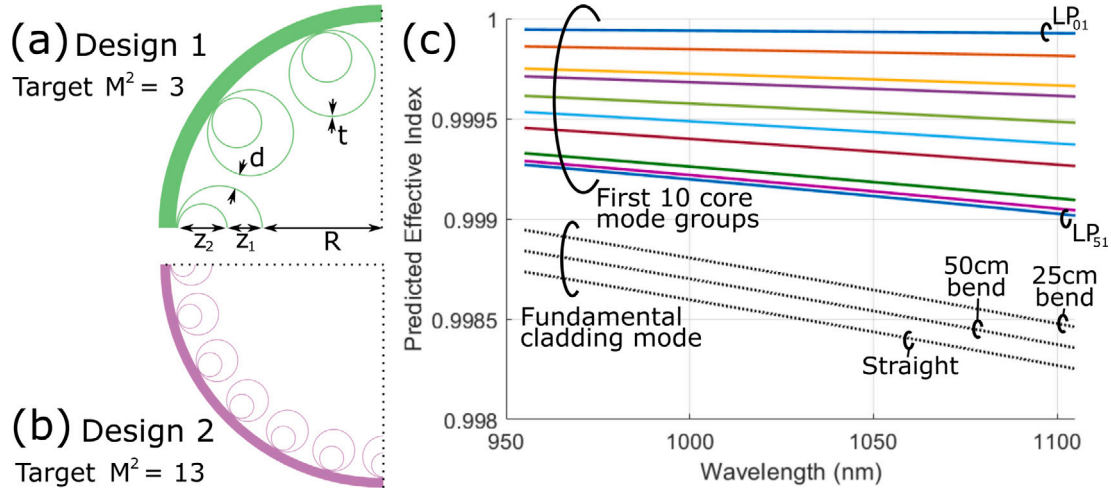
Fig. 5. (a) design 1, a 10-mode-group NANF, (b) design 2, a 62-mode-group NANF and (c) the predicted effective index of the first 10 core mode groups of design 1 using Eq. (9) and the fundamental cladding tube mode when straight and bent using Eqs. (9) and (10).

at 8 cm bend radius [7,52]). In addition to their strong performance theoretically, NANFs are considered a proven design with 100 s of km of single-mode fiber produced in the lab and commercial NANF cables already available and for this reason NANFs shall be focus of the remainder of this work.

To efficiently capture light from sources with $M^2 > 15$ would require a fiber to guide 100+ mode groups. In a NANF, Fig. 4 suggests a core diameter of approximately 300 μm would be required. The significant macro- and micro-bending losses associated with such a large core indicates that NANFs would not be suitable. If it is required to guide a few 100 mode groups in an ARF, the DNANF might be the design of choice. The required core size of a DNANFs is smaller; for example Eq. (8) suggests that 100 low loss mode groups can be guided with a core diameter of less than 150 μm. Additionally DNANFs have even better resilience to bending compared to the NANF [6]. We leave for future work the task of investigating this solution that may be suitable for delivering laser light from highly multi-mode, $M^2 > 15$ sources. In this work we target laser sources with $M^2 < 15$ and therefore limit ourselves to studying NANFs with fewer than 100 mode groups.

3.2. Cladding design

When designing NANFs it is necessary to correctly size the cladding features, each of which guide its own set of cladding air modes, since these strongly impact the loss of the fiber [42]. Single-mode NANFs are designed such that higher-order core modes are strongly coupled to the high-loss cladding modes guided inside the tubes and in the gaps between them, so that the undesired high-order core modes are effectively stripped from the fiber after a short distance of propagation [7]. In a multi-mode NANF, coupling between core and cladding modes must instead be avoided which is achieved by ensuring a sufficiently large separation in effective index between the highest-order core mode and the fundamental mode of the cladding [42].

For this work we developed a technique for designing the cladding of a NANF to achieve multi-mode guidance. The two most significant air regions in the cladding of a NANF are between the outer and nested capillaries and inside the nested ones (marked Z_1 and Z_2 in Fig. 5(a)). Numerical simulations indicate that the effective index of the significant cladding modes are approximately equal when the ratio of the tubes is such that $Z_1/Z_2 = 0.7$ (see geometric definitions in Fig. 5(a)). As well as maximizing the multi-mode potential of the fiber, this assumption simplifies the design since the modes of interest are

guided in the circular air region in the cladding and the quasi-circular core region. The effective index of both the core and cladding modes can therefore be approximated using an analytical determination for the modes of a floating thin-walled capillary (the $N = 1$ structure in Fig. 4) [53]:

$$\text{Re}(n_{\text{eff}}^{(q)}) = n_{\text{air}} - \frac{x_0^2}{2}\left[\frac{1}{n_{\text{air}}}\left(\frac{\lambda}{2\pi R_q}\right)^2 + \frac{1}{n_{\text{air}}^2}\left(\frac{\lambda}{2\pi R_q}\right)^3 \frac{\epsilon_r + 1}{\sqrt{\epsilon_r - 1}}\cot(\phi_{\text{glass}})\right],$$

$$q = \text{core}, \text{cladding} \tag{9}$$

where all variables take their previous meanings. For the cladding mode, $R_{\text{cladding}} = Z_2/2$ is the radius of the nested capillary and $x_0 = 2.405$ (the first zero of the Bessel function $J_0(x)$) corresponding to the fundamental mode. For the core mode $R_{\text{core}} = R$ and x_0 takes the value of the zero of the Bessel function that corresponds to the highest order core mode desired to be guided, see Eq. (8) for the full definition. We note that empirical scaling factors have been reported for the fundamental mode of a tubular fiber to correct for the difference between the geometry of these fibers compared to the floating capillary [54]. We have found, however, that the scaling factor is dependant on the order of the mode and that any additional accuracy is both unnecessary in this application and outweighed by the increased complexity.

Fig. 5(a) shows the geometry of a NANF with $Z_2/Z_1 = 0.7$ and a core radius of 35 μm. The core size is chosen using Fig. 4 to meet the loss requirements previously discussed for a 10 mode group fiber. The size of the nested capillary tube, Z_1 can then be chosen such that phase matching is avoided between the cladding modes and the desired first 10 core modes. The number of outer tubes and inter-tube gap is selected to maintain the core radius without introducing too large gaps, which incur high leakage loss, or too small gaps, which are difficult to fabricate. The fiber in Fig. 5(a) has 10 outer tubes, an inter-tube gap $d = 4$ μm and the nested tube diameter is $Z_1 = 14$ μm. For this geometry, Fig. 5(c) shows the effective index, calculated using Eq. (9), of the first 10 core mode groups (colored solid lines) from the LP_{01} to LP_{51} and of the fundamental cladding tube mode (black dotted line). The effective index decreases for increasing core mode group index. We have found that a phase mismatch of 2×10^{-4} between the effective indices of the core and cladding modes is easily sufficient to avoid strong coupling [42]. The performance of this design will be studied in the next section, here we only report the design process.

It is desirable to ensure in the design phase that bending will not introduce significant losses. This can be also be approximated, prior

to numerical simulation, using a refractive index permutation model for bending. For tolerable bends that do not introduce significantly higher losses, the effective index of the core modes will be approximately unchanged compared to the straight fiber. The effective index of cladding tubes is modified: it is elevated for modes guided in tubes on the outside of the bend (where the optical path length is increased) and reduced for those on the inside. The important value is the largest cladding mode effective index that is on the outside of the bend, which has the smallest phase mismatch with core modes and therefore the strongest coupling. The increased optical path length of this mode can be modeled by modifying the effective refractive index as [52]:

$$n_{\text{air}} = 1 + \frac{R + Z_1 + 2t + 0.5Z_2}{R_{\text{bend}}} \qquad (10)$$

where R_{bend} is the bend radius. Substituting Eq. (10) into Eq. (9) yields an expression for the modified cladding mode effective index. Fig. 5(c) shows the calculated effective index for the fundamental cladding tube mode when straight and under a 25 and 50 cm bend radius. The effective index is increased for a smaller bend radius. Incorporating this calculation into the design allows the fiber to be designed such that strong phase-mismatch and low-loss operation is achieved for the bends required by the targeted application. Fig. 5(c) demonstrates that the minimum phase separation, 2×10^{-4}, is maintained even under a bend of radius 25 cm bend radius and therefore we expect this fiber to be capable of low-loss operation under these conditions.

4. Performance of multi-mode NANF for laser delivery

We designed two fibers at the extremes of the M^2 range of interest to demonstrate our design techniques. The dimensions of Design 1 and Design 2 (shown in Fig. 5) are chosen to deliver power from lasers with $M^2 = 3$ and $M^2 = 13$, respectively. To efficiently capture light from such lasers, Fig. 1 suggests that the fibers are required to guide 10 and 62 mode groups respectively. Using Eq. (9) to avoid coupling to cladding modes we set Z_2 to 7 μm and 6 μm, respectively and $Z_1/Z_2 = 0.7$. We choose a gap size, $d = 4$ μm, comparable to recently fabricated NANFs [4]. With there parameters we find that the minimum core diameter requirement can be met with 10 and 24 tubes for Design 1 and 2, resulting in core diameters of 69 and 176 μm, respectively. We simulated these designs and in the following sections use the results to assess and discuss the suitability of multi-mode NANFs for delivery of high-power lasers in the region of interest.

4.1. Coupling efficiency

When deployed in an industrial environment a fiber will generally adverse conditions such as experience thermal fluctuations and mechanical vibration that will lead to variation in beam focus and alignment at the coupling. Maintaining sufficient coupling efficiency is important since lost power at the coupling will lead to reduced throughput power delivered to the workstation and in extreme cases thermal buildup and damage to the fiber or coupling. Here we study the resilience of MM ARFs when the beam is perturbed from optimal coupling. The coupling efficiency of Design 1 when illuminated by the designed-for $M^2 = 3$ beam at different values of beam waist ratio, w_0/R, is shown in Fig. 6(a). The maximum coupling efficiency is 96%, slightly higher than the 95% target designed for, and occurs for $w_0/R = 0.48$. We model de-focusing of the laser beam as a change in beam waist ratio. Coupling efficiency decreases as the beam waist departs from the optimum but, for Design 1, coupling efficiency remains $\geq 95\%$ for a change in beam waist of $\pm 7\%$. We next consider transverse misalignment; Fig. 6(b) shows how coupling efficiency is impacted as an optimally focused, $w_0/R = 0.48$, $M^2 = 3$ beam incident on Design 1 is offset transversely. Coupling efficiency is maximized when the offset is 0 and the beam is centered on the fiber. As offset

increases the coupling suffers increased insertion loss but the multi-mode nature of the fibers mean these designs are resistant to small transverse misalignment: Fig. 6(b) indicates that, for Design 1, a beam offset by 10% of the core radius still achieves 95% coupling efficiency.

It should be noted that in multi-mode fibers a change of focus or alignment not only alters the total coupling efficiency but also excites the fiber modes differently. Generally a decrease in coupling efficiency also results in a higher fraction of the captured light being coupled into the higher order fiber modes which increases the effective propagation loss of the fiber. In our simulations we have found, however, that input coupling remains the dominant source of loss. For example, after coupling and propagation over 2 km in Design 1, the total loss is less than 0.2 dB greater for a 10% transverse offset compared to an ideal launch with no offset. Propagation losses will be examined further in a Section 4.3.

In Fig. 6(c) and (d) we show the behavior of coupling efficiency with variation in focus and misalignment respectively for Design 2 when illuminated by the targeted $M^2 = 13$ beam. The results are qualitatively very similar to that of Design 1; there is an optimal beam waist and the coupling efficiency decreases with detuning from optimum focus or increasing transverse offset. The maximum coupling efficiency occurs for a beam waist ratio $w_0/R = 0.30$ and is 95%, slightly less than Design 1 whilst still meeting the design target. When the transverse misalignment is 10% of the core radius or the focus is $\pm 5\%$ from optimal, coupling efficiency is 2.5% lower than maximum. The increased higher order mode content of the $M^2 = 13$ beam results in a smaller optimal beam waist ratio, $w_0/R = 0.30$ compared to the $M^2 = 3$ beam used with Design 1. The maximum coupling efficiency and tolerance to misalignment and focus could be improved by guiding more modes in the fiber. Higher coupling efficiency or stronger resilience to misalignment could be built into the calculations shown in Fig. 1 to determine the number of modes required to be guided in order to meet the laser and application requirements.

4.2. Damage threshold for pulsed lasers

In high-power fiber delivery the incident power on the fiber must not damage the fiber. The light induced damage threshold (LIDT) of an ARF is the maximum power it can withstand before the intensity on the glass micro-structure exceeds the LIDT of the fiber material, in this case bulk silica. In this work we take the LIDT of bulk silica to be 100 J/cm^2 at 1030 nm for a 8 ns pulse [57]. Experimental work on microstructured hollow-core fibers suggests that this is a conservative limit, with as much as 3x higher values being reported [19].

The red dashed lines in Fig. 6 show the LIDT of Designs 1 and 2 as a function of the focus and transverse alignment. Due to the low light-glass overlap, the LIDT of the NANFs is well above the power achievable from current CW lasers in the targeted M^2 range and so here we show only the maximum pulse energy of pulsed lasers which produce significantly higher peak powers.

In Fig. 6(a) the maximum 10 ns pulse energy for Design 1 when coupling is optimal is 230 mJ. This corresponds to a maximum peak power of more than 20 MW. The behavior of the LIDT in multi-mode ARF is notably differently to what might be expected in solid-core fibers owing to the fact that the peak optical intensity of the beam is incident on the hollow core and does not damage the microstructure. In Fig. 6(a) the damage threshold increases dramatically as the laser is more tightly focused since this results in a reduction of the intensity incident on the glass. For Design 1 the maximum 10 ns pulse energy at $w_0/R = 0.5$ is 100 mJ, at $w_0/R = 0.45$ it is 500 mJ and at $w_0/R = 0.4$ it is more than 4 J, over 40x higher. We also found that the improvement from higher M^2 beams that have a more flat-top profile was negligible compared to the effect of changing focus. This reveals a route to scale the power-handling capability of MM ARFs by focusing the laser beam to a smaller spot size. The accompanying reduction in coupling efficiency can be acceptable in a MM ARF. This is evident in Fig. 6(a) which shows
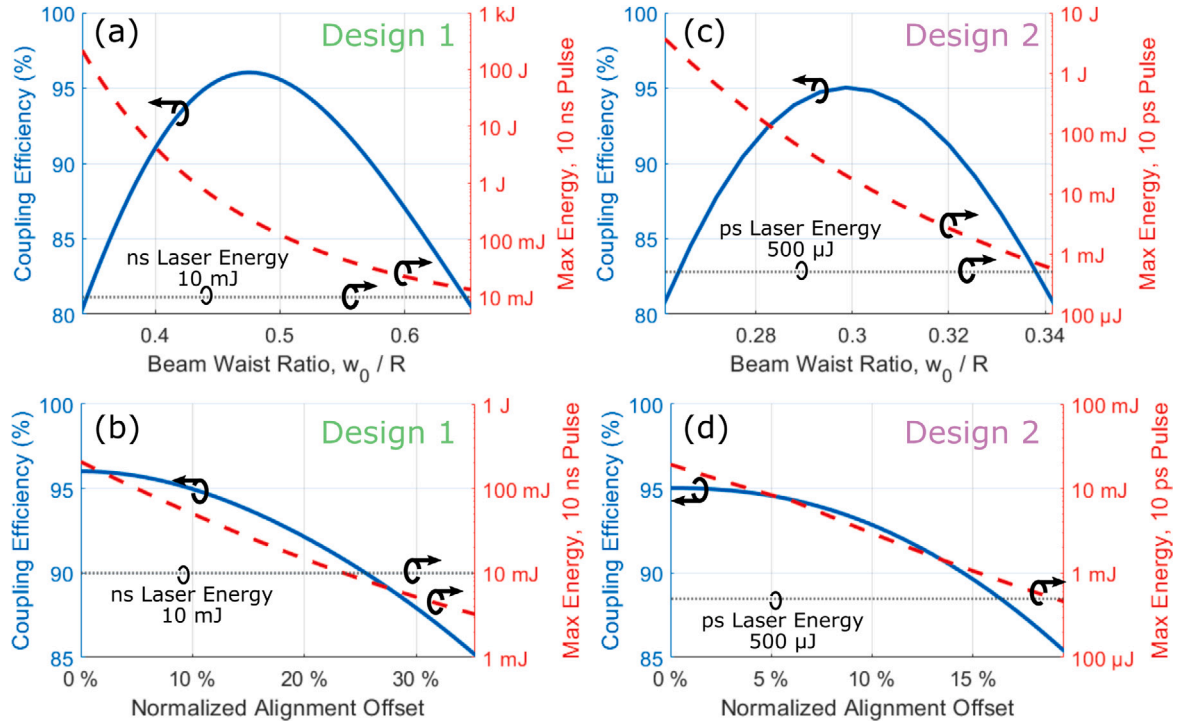
Fig. 6. The coupling efficiency (blue solid) and maximum pulse energy (red dashed) before damage for (a,b) a 10 ns, $M^2 = 3$ pulse incident on Design 1 and (c,d) a 10 ps, $M^2 = 13$ pulse incident on Design 2. The beam is modified by varying (a,c) the beam waist ratio at zero alignment offset or (b,d) the alignment offset at optimal beam waist. Alignment offset is normalized relative to the fiber core radius. The horizontal dotted line indicates the maximum pulse energies of high-energy, commercial nanosecond [55] and picosecond [56] lasers.

that the maximum pulse energy for 10 ns pulses at optimal coupling is 230 mJ but by decreasing the laser focus by just 7%, the coupling is still above 95% but the maximum pulse energy before damage is increased to 650 mJ, almost 3x higher. For comparison with current state-of-the-art, we chose a very high energy nanosecond laser emitting at 1060 nm wavelength with a reported beam M^2 suitable for coupling to this fiber. The commercially available IPG Photonics YLPN has a maximum pulse energy of 10 mJ with a duration of 30 ns and requires a solid-core delivery fiber with a core diameter of 400 μm (more than 5x larger than that of Design 1) [55]. We note that even at optimal coupling the maximum pulse energy is already more than an order of magnitude higher than the YLPN and other typical nanosecond pulse lasers [10]. We also study the maximum energy when Design 2 is illuminated by 10 ps pulses. Fig. 6(c) shows the that the maximum pulse energy before damage at optimal coupling is almost 20 mJ. This is 2 orders of magnitude greater than the commercially-available, high-energy laser chosen for comparison, the Trumpf TruMicro 2070 picosecond laser that has a maximum pulse energy of 500 μJ [56].

Fig. 6(c, d) shows that the damage threshold of ARF lasers decreases as transverse alignment offset increases. This is to be expected given that any transverse offset increases the incident intensity on the glass microstructure. For Design 1 a misalignment of 15% of the core radius results in almost an order of magnitude decrease in damage threshold and in Design 2 the same misalignment reduces the damage threshold by over an order of magnitude. If large misalignment tolerances are required it may be therefore necessary to tighten the laser focus to maintain the damage thresholds.

Given the high damage thresholds compared to current state-of-the-art lasers, we believe that suitably designed MM ARF fibers would be capable of handling the typical powers used in most applications and laser sources currently available, with considerable margins for further laser power up-scale. Having confirmed the suitability for coupling high power lasers into MM ARFs, we next consider their ability to propagate that power.

4.3. Propagation and bending loss

Fig. 7(a) shows leakage loss as a function of wavelength of the highest-order, highest-loss mode of Designs 1 and 2 when straight. The minimum loss of Design 1 is 1.4 dB/km at 1050 nm and, similarly, for Design 2 minimum loss is 0.8 dB/km at 1030 nm. For the chosen wall thickness, 350 nm, the first resonant wavelength is approximately 742 nm and hence loss increases at shorter wavelengths as the first resonance is approached; at 970 nm, leakage loss of both designs is less than 0.3 dB/km higher than their respective minimums. The available bandwidth is suitable for both CW and ultrashort pulsed lasers operating in the 1 μm range (for comparison, the bandwidth of a 100 fs Gaussian pulse at 1064 nm is less than 20 nm). The leakage loss of the highest-order modes as a function of bend radius is shown in Fig. 7(b). In this work bend loss is calculated directly by imposing a conformal transformation to the refractive index in simulation [58]. Loss increases for smaller bend radius. The critical bend radius is the bend radius for which loss is doubled compared to the straight fiber; for Design 2 it is 35 cm and for Design 1 it is less than 25 cm. The similarity between Design 1 and 2 in the dependence of loss with bend radius suggests that the additional bending loss in these designs is primarily due to increased phase matching to cladding modes. When the fiber is bent to a smaller radius, the real component of the effective index of the cladding modes in the tubes on the outside of the bend increases, Eq. (9), whereas the effective index of the core modes is approximately unchanged (smaller bends than those considered here may also modify the effective index of the core modes) [52]. Consequently phase matching is increased between the core and cladding modes and the loss of the core modes increases [42]. Here, both designs demonstrate strong resilience to bending and are below the design threshold of 10 dB/km for bend radii as small as 25 cm radius. This is below the expected minimum bend radius in typical practical environments where the fiber is deployed in a protective cable which limits the mechanical flexibility and we do not expect bend loss to be a limitation in these situations.
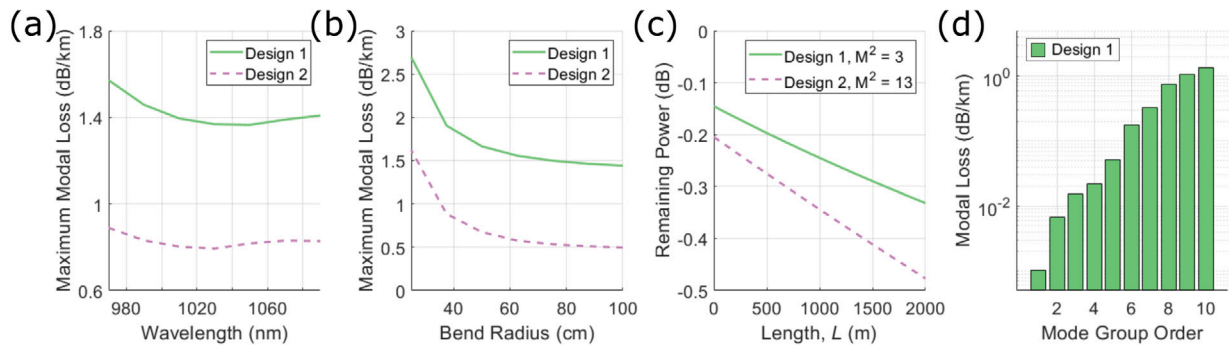
Fig. 7. (a) The maximum modal loss across all modes of Design 1 and 2 when straight. (b) The maximum modal bending loss at 1030 nm across all modes of Designs 1 and 2. (c) Delivered power after coupling and propagation for a $M^2 = 3$ beam incident on Design 1 and a $M^2 = 13$ beam incident on Design 2. Loss values consider a constant 35 cm bend. (d) The maximum leakage loss (blue bar, left axis) and the fraction of power in the glass (red bar, right axis) of all mode groups of Design 1 at 1030 nm when straight.

To understand the throughput capability of the fiber when used in laser delivery Fig. 7(c) shows the delivered output power after coupling and propagation losses. The calculation considers the case of the fibers coiled at a constant 35 cm radius bend when illuminated by the targeted beam: $M^2 = 3$ and $M^2 = 13$ for Design 1 and Design 2 respectively. The initial loss at $L = 0$ is due to insertion loss as discussed in Section 4.1. In these calculations we have not included the effects of scattering losses nor of power coupling between the modes of the fiber. Under these assumptions, after 2 km of propagation the total loss is predicted to be less than 0.5 dB in both designs. Whilst scattering losses are expected to be negligible in such large core NANFs, given such low leakage loss it is reasonable to assume that microbending, which increases rapidly with core size [48], will become the dominant source of propagation loss. The impact of microbending can be reduced or mitigated with choice of fiber packaging [49]. Given the lack of relevant experimental or theoretical data on micro-bending in large-core, multi-mode ARF, however, here we restrict ourselves to studying the effects of differential leakage loss and multi-mode guidance.

We note that the effective leakage loss in Fig. 7(c) is almost an order of magnitude less than the loss of the highest-order mode shown in Fig. 7(b). This is a result of the multi-mode beam coupling which results in a majority of the power being captured in lower-order fiber modes which is demonstrated, for example, in Fig. 2. Fig. 7(d) shows the leakage loss of the first 10 mode groups of Design 1 at a wavelength of 1030 nm. Loss decreases rapidly with decreasing mode order; in Design 1 the leakage loss of the fundamental mode is nearly 3 orders of magnitude lower than that of the highest order mode. Since the majority of power is propagating in the lower order modes, the effective loss of the beam propagating in the fiber is consequently lower than the highest order mode.

We also considered the M^2 of the laser beam at the output of the fiber and found that there was a negligible change compared to the incident beam, due to the extremely low, <0.5 dB, losses. The effects of power coupling between the modes of the fiber may modify the output M^2 [59]. Most applications using such large M^2 sources will be tolerant to small changes in beam quality as measured by M^2. If necessary, the guidance mechanism of ARF does suggest a means of limiting the maximum output M^2. Similar to single-mode ARFs, by designing the fiber such that any undesired modes, those with higher order than the initial design, have high enough losses that any power in those modes will be lost after propagation through the length of the fiber. The output M^2 would therefore be effectively limited by the highest order, low-loss fiber mode. This technique could be used to mitigate the effects of intermodal coupling or indeed to spatially filter the laser source, improving its M^2. As with any filtering technique this would incur additional power loss, however, it may be more desirable to dissipate power in this manner over the length of the fiber rather than in a discrete component at the fiber coupling where it can result

in dangerous heat build-up. We leave for future work the task of investigating this possibility.

4.4. Impact of dispersion on short pulse delivery

The delivery of short pulses requires that we consider the dispersive properties of the fiber, as these may induce significant pulse broadening, thus distorting the temporal profile and lowering the output peak instantaneous power. Although single-mode ARFs generally have lower dispersion compared to their solid-core counterparts, the dispersion increases for higher-order modes. Furthermore, when operating in a few-mode or multi-mode regime, the effect of intermodal differential group delay (DGD) must also be considered. In ARFs, both dispersion and DGD increase approximately linearly with mode order but are decreased for larger cores [45]. Fig. 8 shows the chromatic dispersion and DGD of the highest order modes of Designs 1 and 2 in the bandwidth of interest. Although Design 2 guides 6x more modes than Design 1, the larger core size required to achieve similar loss also results in similar values of maximum DGD and dispersion in the highest order modes. Fig. 8(c) shows the DGD of the modes of Design 2 (note that we show only every tenth mode for clarity of reading). The DGD of the 60th mode is 7x that of the 10th mode. Given such strong differential modal properties, the dispersion experienced by a short pulse will strongly depend on the exact modal power distribution after the laser coupling and on the rate of intermodal power coupling along the length of the fiber. Both of these factors are highly dependent on the environmental conditions and would be difficult to predict with any accuracy without more experimental data involving large-core multi-mode ARFs. Here, we therefore only consider the case of completely uncoupled modes with 100% power propagating in the highest-order mode (or when studying DGD: 50% in the highest-order and 50% in the fundamental mode). Whilst very unrealistic, this describes an absolute worst-case scenario and serves to illustrate where further research may be necessary. The true performance of multi-mode ARFs for delivering short pulses is likely to be significantly better than what is described here.

We consider the two cases described in Section 4.1: 10 ns pulses propagating in Design 1 and 10 ps pulses propagating in Design 2. The dispersion length, $L_D = \frac{2\pi c_0}{\lambda^2} \frac{\tau_0^2}{|D|}$, for an initially unchirped, temporally-Gaussian pulse of duration τ_0 propagating in a waveguide with dispersion D, is defined as the distance over which the duration of that pulse increases by a factor of $\sqrt{2}$. The dispersion length is over 3 km for a 10 ps pulse in Design 2 whilst for a 10 ns pulse the value is 6 orders of magnitude larger. Clearly, chromatic dispersion will have a negligible impact on propagation.

A quantity similar to the dispersion length for chromatic dispersion can also be calculated for DGD. We define the DGD dispersion length, $L_{DGD} = \frac{\tau_0(\sqrt{2}-1)}{|DGD|}$ for a square wave of duration τ_0 with 50% of power in
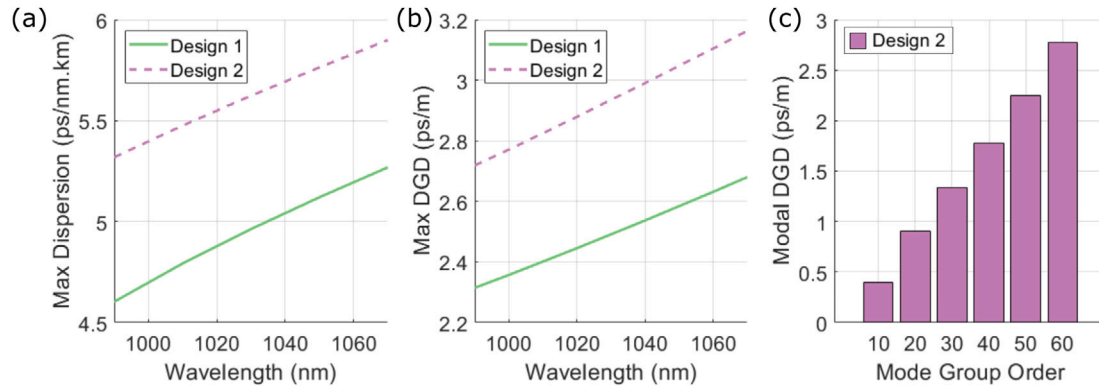
Fig. 8. For the highest order modes of Design 1 and 2 (a) the dispersion parameter, D, and (b) the differential group delay as a function of wavelength. (c) the DGD of every tenth mode group in Design 2 at 1030 nm.

the fundamental fiber mode and 50% power in the highest order mode as the distance over which the duration of that pulse increases by a factor $\sqrt{2}$. These fibers have moderate resilience to nanosecond pulses; a 10 ns pulse propagating in Design 1 has $L_{DGD} = 1.7$ km. Ultrafast pulses, however, are strongly impacted: a 10 ps pulse propagating in Design 2 has $L_{DGD} = 1.4$ m. Although this is a worst-case scenario estimation, we believe that, without mitigation techniques, DGD will be the limiting factor for delivering high-power, low-beam-quality pulses of picosecond duration in MM ARFs. The DGD can be reduced in ARF by increasing the size of the core or by reducing the number of modes in which power is guided (see Fig. 8(c)). Current picosecond duration pulsed lasers generally have lower M^2 values than what we have so far assumed; if we instead consider a 10 ps pulse with $M^2 = 3$, very similar to [32], then more than 95% of the power is coupled into the first 10 mode groups. Taking the DGD as that of the tenth mode group then $L_{DGD} = 10.5$ m which is comparable to the maximum lengths of typical solid-core power-delivery fiber. Despite the high DGD compared to multi-mode, solid-core, graded-index fibers, MM NANF permits order of magnitude higher damage thresholds and more flexible fibers due to the low bending loss, less than 2.5 dB/km at 35 cm bend radius, and smaller core size, e.g. Design 1 has a 5x smaller core than comparable fibers for nanosecond delivery [55].

5. Conclusions

In this work we have presented a simple, effective technique for the design of multi-mode NANFs for delivering power from high-power, multi-mode laser sources. Using this technique we designed and simulated two fibers targeting beams characterized by $M^2 = 3$ and 13 respectively. The theoretical coupling efficiency of both fibers to their multi-mode laser inputs is >95% coupling efficiency and both can deliver power with negligible leakage loss whilst tolerating bends with radii under 35 cm and seem capable of multi-km flexible laser delivery with little loss. All the requirements imposed by our design technique were met and we discussed how it could be extended further e.g. to include beam misalignment tolerance.

The damage threshold of the fibers considered here are between 20x and 40x greater than typical requirements of high-intensity nanosecond and picosecond pulses and can be increased significantly further if the fibers are designed to guide more modes. The DGD of the highest order modes is likely to limit the reach of picosecond pulses to several metres but we believe this can be mitigated by increasing the core size, although this may reduce the fiber's resilience to bending

The potential of these fibers to deliver 10 s of kW power over multi-km distances presents several opportunities in novel as well as existing applications. For example in situations where the laser

processing target is difficult or hazardous to access such as nuclear decommissioning [60], or for subsurface rock drilling for the extraction of gas and oil [61]. Equally, in existing factory machining applications, such long distance delivery offers greater flexibility; high-power lasers, and their associated power and cooling requirements which are often significant, could be physically removed from the production line.

Our work demonstrates that MM ARFs are capable of delivering energy from high-power laser sources with large M^2 beams over significantly larger distances and with greater power damage thresholds than current solid-core fibers and do so with similar or improved flexibility.

CRediT authorship contribution statement

William Shere: Conceptualization, Methodology, Investigation, Writing – original draft. **Gregory T. Jasion:** Conceptualization, Methodology, Writing – review & editing. **Eric Numkam-Fokoua:** Conceptualization, Methodology, Writing – review & editing. **Francesco Poletti:** Conceptualization, Writing – review & editing, Supervision.

Declaration of competing interest

The authors declare that they have no known competing financial interests or personal relationships that could have appeared to influence the work reported in this paper.

Data availability

Data will be made available on request.

References

[1] F. Yu, J.C. Knight, Negative curvature hollow-core optical fiber, IEEE J. Sel. Top. Quantum Electron. 22 (2) (2016) http://dx.doi.org/10.1109/JSTQE.2015.2473140.

[2] G.T. Jasion, T. Bradley, H. Sakr, J.R. Hayes, Y. Chen, A. Taranta, H.C. Mulvad, I.A. Davidson, N.V. Wheeler, E.N. Fokoua, W. Wang, D.J. Richardson, F. Poletti, Recent breakthroughs in hollow core fiber technology, in: Proc.SPIE, Vol. 11309, 2020, http://dx.doi.org/10.1117/12.2548585.

[3] A.D. Pryamikov, A.S. Biriukov, A.F. Kosolapov, V.G. Plotnichenko, S.L. Semjonov, E.M. Dianov, Demonstration of a waveguide regime for a silica hollow - core microstructured optical fiber with a negative curvature of the core boundary in the spectral region > 3.5 μm, Opt. Express 19 (2) (2011) 1441–1448, http://dx.doi.org/10.1364/OE.19.001441.

[4] G.T. Jasion, T.D. Bradley, K. Harrington, H. Sakr, Y. Chen, E.N. Fokoua, I.A. Davidson, A. Taranta, J.R. Hayes, D.J. Richardson, F. Poletti, Hollow core NANF with 0.28 dB/km attenuation in the C and L bands, in: Optical Fiber Communication Conference Postdeadline Papers 2020, Optical Society of America, San Diego, California, 2020, p. Th4B.4, http://dx.doi.org/10.1364/OFC.2020.Th4B.4.

[5] H. Sakr, T.D. Bradley, G.T. Jasion, E.N. Fokoua, S.R. Sandoghchi, I.A. Davidson, A. Taranta, G. Guerra, W. Shere, Y. Chen, J.R. Hayes, D.J. Richardson, F. Poletti, Hollow core NANFs with five nested tubes and record low loss at 850, 1060, 1300 and 1625 nm, in: 2021 Optical Fiber Communications Conference and Exhibition (OFC), 2021, pp. 1–3.

[6] G.T. Jasion, H. Sakr, J.R. Hayes, S.R. Sandoghchi, L. Hooper, E.N. Fokoua, A. Saljoghei, H.C. Mulvad, M. Alonso, A. Taranta, T.D. Bradley, I.A. Davidson, Y. Chen, D.J. Richardson, F. Poletti, 0.174 dB/km hollow core double nested antiresonant nodeless fiber (DNANF), in: 2022 Optical Fiber Communications Conference and Exhibition (OFC), 2022, pp. 1–3.

[7] F. Poletti, Nested antiresonant nodeless hollow core fiber, Opt. Express 22 (20) (2014) 23807, http://dx.doi.org/10.1364/OE.22.023807.

[8] A. Taranta, E. Numkam Fokoua, S. Abokhamis Mousavi, J.R. Hayes, T.D. Bradley, G.T. Jasion, F. Poletti, Exceptional polarization purity in antiresonant hollow-core optical fibres, Nat. Photonics 14 (8) (2020) 504–510, http://dx.doi.org/10.1038/s41566-020-0633-x.

[9] V. Michaud-Belleau, E. Numkam Fokoua, T.D. Bradley, J.R. Hayes, Y. Chen, F. Poletti, D.J. Richardson, J. Genest, R. Slavík, Backscattering in antiresonant hollow-core fibers: over 40 dB lower than in standard optical fibers, Optica 8 (2) (2021) 216–219, http://dx.doi.org/10.1364/OPTICA.403087.

[10] D.J. Richardson, J. Nilsson, W.A. Clarkson, High power fiber lasers: current status and future perspectives [Invited], J. Opt. Soc. Amer. B 27 (11) (2010) B63–B92, http://dx.doi.org/10.1364/JOSAB.27.000B63.

[11] J.W. Dawson, M.J. Messerly, R.J. Beach, M.Y. Shverdin, E.A. Stappaerts, A.K. Sridharan, P.H. Pax, J.E. Heebner, C.W. Siders, C.P.J. Barty, Analysis of the scalability of diffraction-limited fiber lasers and amplifiers to high average power, Opt. Express 16 (17) (2008) 13240–13266, http://dx.doi.org/10.1364/OE.16.013240.

[12] C. Rohrer, C.A. Codemard, G. Kleem, T. Graf, M.A. Ahmed, Preserving nearly diffraction-limited beam quality over several hundred meters of transmission through highly multimode fibers, J. Lightwave Technol. 37 (17) (2019) 4260–4267, http://dx.doi.org/10.1109/JLT.2019.2922776.

[13] T. Okuda, Y. Fujiya, S. Goya, A. Inoue, Beam transmission technology by photonic crystal fiber to realizes high-precision and high-efficiency laser processing technology, Mitsubishi Heavy Ind. Tech. Rev. 57 (2020) 1–5.

[14] IPG photonics YLS, 2022, https://www.ipgphotonics.com/en/products/lasers/high-power-cw-fiber-lasers/1-micron/yls-1-120-kw. Accessed 4- Jul- 2022.

[15] F. Couny, F. Benabid, P.S. Light, Large-pitch kagome-structured hollow-core photonic crystal fiber, Opt. Lett. 31 (24) (2006) 3574–3576, http://dx.doi.org/10.1364/OL.31.003574.

[16] S.A. Mousavi, H.C.H. Mulvad, N.V. Wheeler, P. Horak, J. Hayes, Y. Chen, T.D. Bradley, S.-u. Alam, S.R. Sandoghchi, E.N. Fokoua, D.J. Richardson, F. Poletti, Nonlinear dynamic of picosecond pulse propagation in atmospheric air-filled hollow core fibers, Opt. Express 26 (7) (2018) 8866–8882, http://dx.doi.org/10.1364/OE.26.008866.

[17] L.F. Michaille, D.M. Taylor, C.R.H. Bennett, T.J. Shepherd, C. Jacobsen, T.P. Hansen, Damage threshold and bending properties of photonic crystal and photonic band-gap optical fibers, in: Proc.SPIE, Vol. 5618, 2004, http://dx.doi.org/10.1117/12.583481.

[18] B. Beaudou, F. Gérôme, Y.Y. Wang, M. Alharbi, T.D. Bradley, G. Humbert, J.-L. Auguste, J.-M. Blondy, F. Benabid, Millijoule laser pulse delivery for spark ignition through kagome hollow-core fiber, Opt. Lett. 37 (2012) 1430–1432, http://dx.doi.org/10.1364/OL.37.001430.

[19] P. Jaworski, F. Yu, R.R.J. Maier, W.J. Wadsworth, J.C. Knight, J.D. Shephard, D.P. Hand, Picosecond and nanosecond pulse delivery through a hollow-core negative curvature fiber for micro-machining applications, Opt. Express 21 (19) (2013) 22742–22753, http://dx.doi.org/10.1364/OE.21.022742.

[20] M. Michieletto, J.K. Lyngsø, C. Jakobsen, J. Lægsgaard, O. Bang, T.T. Alkeskjold, Hollow-core fibers for high power pulse delivery, Opt. Express 24 (7) (2016) 7103–7119, http://dx.doi.org/10.1364/OE.24.007103.

[21] S. Eilzer, B. Wedel, Hollow core optical fibers for industrial ultra short pulse laser beam delivery applications, 2018, http://dx.doi.org/10.3390/fib6040080.

[22] Q. Fu, Y. Wu, I.A. Davidson, L. Xu, G.T. Jasion, S. Liang, S. Rikimi, F. Poletti, N.V. Wheeler, D.J. Richardson, Hundred-meter-scale, kilowatt peak-power, near-diffraction-limited, mid-infrared pulse delivery via the low-loss hollow-core fiber, Opt. Lett. 47 (20) (2022) 5301–5304, http://dx.doi.org/10.1364/OL.473230.

[23] H.C.H. Mulvad, S. Abokhamis Mousavi, V. Zuba, L. Xu, H. Sakr, T.D. Bradley, J.R. Hayes, G.T. Jasion, E. Numkam Fokoua, A. Taranta, S.-U. Alam, D.J. Richardson, F. Poletti, Kilowatt-average-power single-mode laser light transmission over kilometre-scale hollow-core fibre, Nat. Photonics 16 (6) (2022) 448–453, http://dx.doi.org/10.1038/s41566-022-01000-3.

[24] U. Brauch, C. Röcker, T. Graf, M. Abdou Ahmed, High-power, high-brightness solid-state laser architectures and their characteristics, Appl. Phys. B: Lasers Opt. 128 (3) (2022) 1–32, http://dx.doi.org/10.1007/s00340-021-07736-0.

[25] V. Kuhn, T. Gottwald, C. Stolzenburg, S.-S. Schad, A. Killi, T. Ryba, Latest advances in high brightness disk lasers, Solid State Lasers XXIV: Technol. Devices 9342 (2015) 216–222, http://dx.doi.org/10.1117/12.2079876.

[26] S. Nagel, B. Metzger, T. Gottwald, V. Kuhn, A. Killi, S.S. Schad, Thin disk laser operating in fundamental mode up to a power of 4 kW, in: 2019 Conference on Lasers and Electro-Optics Europe and European Quantum Electronics Conference, CLEO/Europe-EQEC 2019, 2019, http://dx.doi.org/10.1109/CLEOE-EQEC.2019.8872516.

[27] A. Diebold, C.J. Saraceno, C.R. Phillips, F. Saltarelli, I.J. Graumann, U. Keller, Gas-lens effect in kW-class thin-disk lasers, Opt. Express 26 (10) (2018) 12648–12659, http://dx.doi.org/10.1364/OE.26.012648.

[28] R. Fleischhaker, R. Gebs, A. Budnicki, M. Wolf, J. Kleinbauer, D.H. Sutter, Compact gigawatt-class sub-picosecond Yb:YAG thin-disk regenerative chirped-pulse amplifier with high average power at up to 800 kHz, in: 2013 Conference on Lasers and Electro-Optics Europe and International Quantum Electronics Conference, CLEO/Europe-IQEC 2013, 2013.

[29] D. Sutter, F. Krausz, M. Ueffing, R. Lange, T. Metzger, T. Nubbemeyer, T. Pleyer, V. Pervak, Z. Major, Direct regenerative amplification of femtosecond pulses to the multimillijoule level, Opt. Lett. 41 (16) (2016) 3840–3843, http://dx.doi.org/10.1364/OL.41.003840, Vol. 41, Issue 16, pp. 3840-3843.

[30] O.H. Heckl, J. Kleinbauer, D. Bauer, S. Weiler, T. Metzger, D.H. Sutter, Ultrafast thin-disk lasers, Springer Ser. Optical Sci. 195 (2016) 93–115.

[31] C. Herkommer, P. Krötz, R. Jung, S. Klingebiel, C. Wandt, R. Bessing, P. Walch, T. Produit, K. Michel, D. Bauer, R. Kienberger, T. Metzger, Ultrafast thin-disk multipass amplifier with 720 mj operating at kilohertz repetition rate for applications in atmospheric research, Opt. Express 28 (20) (2020) 30164–30173, http://dx.doi.org/10.1364/OE.404185, Vol. 28, Issue 20, pp. 30164-30173.

[32] A. Loescher, C. Röcker, M.A. Ahmed, T. Graf, Azimuthally polarized picosecond vector beam with 1.7 kW of average output power, Opt. Lett. 46 (14) (2021) 3492–3495, http://dx.doi.org/10.1364/OL.431995, Vol. 46, Issue 14, pp. 3492-3495.

[33] T. Dietz, M. Jenne, D. Bauer, M. Scharun, D. Sutter, A. Killi, Ultrafast thin-disk multi-pass amplifier system providing 1.9 kW of average output power and pulse energies in the 10 mJ range at 1 ps of pulse duration for glass-cleaving applications, Opt. Express 28 (8) (2020) 11415–11423, http://dx.doi.org/10.1364/OE.383926, Vol. 28, Issue 8, pp. 11415-11423.

[34] H.D. Hoffmann, J. Weitenberg, P. Russbueldt, R. Poprawe, T. Mans, Compact diode-pumped 1.1 kW Yb:YAG innoslab femtosecond amplifier, Opt. Lett. 35 (24) (2010) 4169–4171, http://dx.doi.org/10.1364/OL.35.004169, Vol. 35, Issue 24, pp. 4169-4171.

[35] P. Russbueldt, D. Hoffmann, M. Höfer, J. Löhring, J. Luttmann, A. Meissner, J. Weitenberg, M. Traub, T. Sartorius, D. Esser, R. Wester, P. Loosen, R. Poprawe, Innoslab amplifiers, IEEE J. Sel. Top. Quantum Electron. 21 (1) (2015) 447–463, http://dx.doi.org/10.1109/JSTQE.2014.2333234.

[36] B.E. Schmidt, A. Hage, T. Mans, F. Legare, H.J. Worner, Highly stable, 54 mJ Yb-InnoSlab laser platform at 0.5 kW average power, Opt. Express 25 (15) (2017) 17549–17555, http://dx.doi.org/10.1364/OE.25.017549, Vol. 25, Issue 15, pp. 17549-17555.

[37] J. Sun, L. Liu, L. Han, Q. Zhu, X. Shen, K. Yang, 100 kW ultra high power fiber laser, Opt. Continuum 1 (9) (2022) 1932–1938, http://dx.doi.org/10.1364/OPTCON.465836.

[38] TRUMPF | TruDisk, 2022, https://www.trumpf.com/en_INT/products/laser/disk-lasers/trudisk/. Accessed 4- Jul- 2022..

[39] IPG photonics YLS-SM, 2022, https://www.ipgphotonics.com/en/products/lasers/high-power-cw-fiber-lasers/1-micron/yls-sm-1-10-kw. Accessed 4- Jul-2022..

[40] TRUMPF | TruPulse, 2022, https://www.trumpf.com/en_GB/products/laser/pulsed-lasers/trupulse/. Accessed 4- Jul- 2022..

[41] A.E. Siegman, Defining, measuring, and optimizing laser beam quality, in: Proc.SPIE, Vol. 1868, 1993, http://dx.doi.org/10.1117/12.150601.

[42] W. Shere, G.T. Jasion, E. Numkam Fokoua, F. Poletti, Understanding the impact of cladding modes in multi-mode hollow-core anti-resonant fibres, Opt. Fiber Technol., Mater. Devices Syst. 71 (2022) 102919, http://dx.doi.org/10.1016/j.yofte.2022.102919.

[43] V. Zuba, H.C.H. Mulvad, R. Slavík, H. Sakr, F. Poletti, D.J. Richardson, E.N. Fokoua, Experimental investigation into optimum laser coupling efficiency into hollow-core NANFs, in: Conference on Lasers and Electro-Optics, in: Technical Digest Series, Optica Publishing Group, San Jose, California, 2022, p. SW4K.1.

[44] A.E. Siegman, New developments in laser resonators, in: Proc.SPIE, Vol. 1224, 1990, http://dx.doi.org/10.1117/12.18425.

[45] E.A.J. Marcatili, R.A. Schmeltzer, Hollow metallic and dielectric waveguides for long distance optical transmission and lasers, Bell Syst. Tech. J. 43 (4) (1964) 1783–1809.

[46] E.N. Fokoua, R. Slavik, D.J. Richardson, F. Poletti, Limits of coupling efficiency into hollow-core antiresonant fibers, in: 2021 Conference on Lasers and Electro-Optics (CLEO), 2021, pp. 1–2.

[47] J.R. Hayes, F. Poletti, M.S. Abokhamis, N.V. Wheeler, N.K. Baddela, D.J. Richardson, Anti-resonant hexagram hollow core fibers, Opt. Express 23 (2) (2015) 1289, http://dx.doi.org/10.1364/OE.23.001289.

[48] E.N. Fokoua, Y. Chen, D.J. Richardson, F. Poletti, Microbending effects in hollow-core photonic bandgap fibers, in: ECOC 2016; 42nd European Conference on Optical Communication, 2016, pp. 1–3.

[49] E. Numkam Fokoua, S. Abokhamis Mousavi, G.T. Jasion, D.J. Richardson, F. Poletti, Loss in hollow-core optical fibers: mechanisms, scaling rules, and limits, Advances in Optics and Photonics 15 (1) (2023) 1–85, http://dx.doi.org/10.1364/AOP.470592.

[50] D. Bird, Attenuation of model hollow-core, anti-resonant fibres, Opt. Express 25 (19) (2017) 23215, http://dx.doi.org/10.1364/OE.25.023215.

[51] B. Winter, T.A. Birks, W.J. Wadsworth, Multimode hollow-core anti-resonant optical fibres, in: Frontiers in Optics + Laser Science APS/DLS, in: The Optical Society, Optical Society of America, Washington, DC, 2019, p. JTu4A.18.

[52] M.H. Frosz, P. Roth, M.C. Günendi, P.S. Russell, Analytical formulation for the bend loss in single-ring hollow-core photonic crystal fibers, Photonics Res. 5 (2) (2017) 88–91, http://dx.doi.org/10.1364/PRJ.5.000088.

[53] M. Zeisberger, M.A. Schmidt, Analytic model for the complex effective index of the leaky modes of tube-type anti-resonant hollow core fibers, Sci. Rep. 7 (1) (2017) 11761, http://dx.doi.org/10.1038/s41598-017-12234-5.

[54] P. Uebel, M.C. Günendi, M.H. Frosz, G. Ahmed, N.N. Edavalath, J.-M. Ménard, P.S. Russell, Broadband robustly single-mode hollow-core PCF by resonant filtering of higher-order modes, Opt. Lett. 41 (9) (2016) 1961–1964, http://dx.doi.org/10.1364/OL.41.001961.

[55] IPG photonics YLPN 1-10 mJ, 100-300 W, 2022, https://www.ipgphotonics.com/en/products/lasers/nanosecond-fiber-lasers/1-06-micron/ylpn-1-2-mj-100-300-w. Accessed 7- Jul- 2022.

[56] TRUMPF │ TruMicro series 2000, 2022, https://www.trumpf.com/en_GB/products/laser/short-and-ultrashort-pulse-lasers/trumicro-series-2000/. Accessed 7- Jul- 2022.

[57] F. Rainer, L.J. Atherton, J.H. Campbell, F.P.D. Marco, M.R. Kozlowski, A.J. Morgan, M.C. Staggs, Four-harmonic database of laser-damage testing, in: Proc.SPIE, Vol. 1624, 1992, http://dx.doi.org/10.1117/12.60128.

[58] M. Heiblum, J. Harris, Analysis of curved optical waveguides by conformal transformation, IEEE J. Quantum Electron. 11 (2) (1975) 75–83, http://dx.doi.org/10.1109/JQE.1975.1068563.

[59] M.A. Cooper, S. Wittek, D. Cruz-Delgado, J. Wahlen, J.M. Mercado, J.E. Antonio-Lopez, R.A. Correa, Higher order mode generation in an anti-resonant hollow-core fiber, in: Proc.SPIE, Vol. 11724, 2021, http://dx.doi.org/10.1117/12.2587936.

[60] P.A. Hilton, A. Khan, Underwater cutting using a 1 μm laser source, J. Laser Appl. 27 (3) (2015) 032013, http://dx.doi.org/10.2351/1.4922384.

[61] M.S. Zediker, High power fiber lasers in geothermal, oil and gas, in: Proc.SPIE, Vol. 8961, 2014, http://dx.doi.org/10.1117/12.2042339.